Articles you may be interested in

Interatomic Coulombic decay following resonant core excitation of Ar in argon dimer
J. Chem. Phys. **141**, 064307 (2014); 10.1063/1.4891986

Interatomic Coulombic decay and its dynamics in NeAr following K - L L Auger transition in the Ne atom
J. Chem. Phys. **131**, 104303 (2009); 10.1063/1.3211114

Ab initio investigation of the autoionization process Ar * (4 s P 2 3 , P 0 3) + Hg → (Ar – Hg) + + e − : Potential energy curves and autoionization widths, ionization cross sections, and electron energy spectra
J. Chem. Phys. **122**, 184309 (2005); 10.1063/1.1891666

An ab initio potential energy surface and predissociative resonances of HArF
J. Chem. Phys. **120**, 4273 (2004); 10.1063/1.1643714

Auger decay of the C 1s −1 2π * resonance in carbon monoxide: Vibrationally and angularly resolved spectra
J. Chem. Phys. **111**, 9642 (1999); 10.1063/1.480337

The effect of the partner atom on the spectra of interatomic Coulombic decay triggered by resonant Auger processes

T. Miteva,[1,a)] Y.-C. Chiang,[1] P. Kolorenč,[2] A. I. Kuleff,[1] L. S. Cederbaum,[1] and K. Gokhberg[1]

[1]*Theoretische Chemie, Physikalisch-Chemisches Institut, Universität Heidelberg, Im Neuenheimer Feld 229, D-69120 Heidelberg, Germany*
[2]*Institute of Theoretical Physics, Faculty of Mathematics and Physics, Charles University in Prague, V Holešovičkách 2, 180 00, Prague, Czech Republic*

The resonant-Auger – interatomic Coulombic decay (ICD) cascade was recently suggested as an efficient means of controlling the course of the ICD process. Recent theoretical and experimental works show that control over the energies of the emitted ICD electrons can be achieved either by varying the photon energy to produce different initial core excitations or by changing the neighboring species. This work presents a theoretical investigation on the role of the rare-gas neighbor and clarifies how the latter influences the ICD process. For this purpose, we compare fully *ab initio* computed ICD-electron and kinetic energy release spectra following the $2p_{3/2} \rightarrow 4s$, $2p_{1/2} \rightarrow 4s$ and $2p_{3/2} \rightarrow 3d$ of Ar in ArKr and Ar$_2$. We demonstrate that the presence of the chemically "softer" partner atom results in an increase in the energies of the emitted ICD electrons, and also in the appearance of additional ICD-active states. The latter leads to a threefold increase in the ICD yield for the case of the $2p_{3/2, 1/2} \rightarrow 4s$ parent core excitations. © *2014 AIP Publishing LLC.*
[http://dx.doi.org/10.1063/1.4898154]

I. INTRODUCTION

Excited electronic states of atoms and molecules may de-excite by ionizing the medium in a relaxation pathway termed interatomic/intermolecular Coulombic decay (ICD). Since its theoretical prediction in 1997,[1] ICD has been the subject of numerous theoretical and experimental studies (see, e.g., Refs. 2 and 3), exploring both the interatomic and intermolecular decay initiated by different kinds of ionizing radiation. The initial ICD states can be produced either directly by photoexcitation, photoionization, electron or ion impact,[4] or as a result of a complex decay cascade.[5–7] In a recent publication,[8] a scheme for achieving site-selectivity as well as control over the energies of the emitted slow electrons was suggested. It exploits the properties of resonant core excitation followed by the resonant-Auger – ICD (RA–ICD) cascade. The aforementioned mechanism was experimentally demonstrated in a variety of rare-gas and molecular dimers such as ArNe, Ar$_2$, ArKr, ArXe,[9–11] (CO)$_2$, and (N$_2$)$_2$.[12]

We have recently computed ICD spectra arising from the RA–ICD cascade in the homonuclear rare-gas dimer Ar$_2$.[13] Our results were in good agreement with the experimental data.[10,14] Detailed analysis of the cascade showed that the large number of initial ICD states can be divided into two groups having different decay dynamics. The group of the fast-decaying states comprises the lowest satellites (i.e., the states of 2h1p character populated in the resonant Auger decay), for which the electronic decay outpaces the typical vibrational motion. The decay of these states occurs around the ground-state equilibrium distance R_e since no significant nuclear motion takes place. The group of the slow-decaying states includes the higher-lying satellites, whose ICD lifetimes are much longer than the characteristic vibrational periods. Therefore, the ICD of these states is accompanied by nuclear motion and occurs predominantly at the inner turning point of the corresponding satellite potential energy curve (PEC).

The structure of the ICD-electron and kinetic energy release (KER) spectra depends not only on the specific manifold of decaying states, but also on the nature of the neighboring species. This sensitivity of the spectra has been employed for spectroscopic characterization of large mixed rare-gas clusters.[15,16] Experimental studies of the role of the partner atom in the RA–ICD cascade confirm that the partner atom's nature can influence the ICD emission[11] and, moreover, that it can serve as a switch for particular decay channels.[9] In this paper, we clarify what effect the presence of a chemically "softer" neighbor has on the ICD spectra. To this end, we computed *ab initio* the ICD spectra of ArKr produced in the RA–ICD cascade following the $2p_{3/2} \rightarrow 4s$, $2p_{1/2} \rightarrow 4s$, and $2p_{3/2} \rightarrow 3d$ core excitations of Ar and compared them with the corresponding spectra of Ar$_2$. We also compared our theoretical results with the available experimental data[11,14] and with the spectra in Ref. 8 obtained using a simple model of the cascade.

The paper is organized as follows: in Sec. II we present the computational details for obtaining the PECs of the states involved in the cascade and the corresponding decay widths used for performing the nuclear dynamics calculations. In Sec. III, we discuss the influence of the partner atom on the PECs and the decay widths, as well as on the computed

a)Electronic mail: tsveta.miteva@pci.uni-heidelberg.de

ICD-electron and KER spectra. The conclusions are given in Sec. IV.

II. COMPUTATIONAL DETAILS

In this section, we only briefly outline the computational approaches used for obtaining the ICD-electron and KER spectra. A more detailed explanation of the calculations is given in Ref. 13. Assuming instantaneous excitation and resonant Auger steps, significant nuclear dynamics take place only during the ICD step. Therefore, the PECs needed for the accurate description of the dynamics are the ground state, the ionized-excited states of the kind $Ar^+(3p^{-2}nl)Kr$, and the final two-site dicationic states $Ar^+(3p^{-1})Kr^+(4p^{-1})$.

The ground-state PEC was computed using the coupled-cluster singles, doubles, and perturbative triples (CCSD(T)) method as implemented in the GAMESS-US suite of programs.[17,18] The aug-cc-pV5Z basis set[19,20] was used on both atoms and its most diffuse s, p, d, f, and g functions were also added at the midpoint position. The ionization satellites of ArKr were computed using the configuration interaction (CI) method as implemented in the GAMESS-US computational package[21,22] with the configuration space comprising all single and double excitations from the reference configuration (CISD). The basis set on Ar was cc-pVDZ[19] augmented with four diffuse s and d, and two compact d functions.[23] The aug-cc-pVTZ basis set[20] was used on Kr. The PECs of the one-site and the two-site dicationic states were computed using the same method, basis set and computational package as used for the ionization satellites. Similar to Ar_2, it was computationally impossible to obtain some of the higher-lying Rydberg states due to the large number of roots of the CI matrix needed, as well as the high density of states in the energy range of interest. We have shown[24] that the respective PECs can be fairly accurately reproduced by the PECs of the corresponding parent dicationic states. Therefore, the PECs of the $Ar^+(3p^{-2}4d)Kr$ states, which form approximately 30% of the satellites populated in the decay of the $2p_{3/2} \rightarrow 3d$ core excitation, were approximated by averages of the PECs of the parent $Ar^{++}(3p^{-2})$ Kr dicationic states. At asymptotic distances, the PECs of the ionization satellites and two-site dicationic final states were adjusted to the corresponding sums of atomic energies taken from the NIST database.[25] The NIST energies were averaged over all possible fine-structure components since the spin-orbit coupling was not accounted for in our calculations. As discussed in Ref. 24, the error resulting from the lack of size-consistency of the CISD method is small for the investigated system and depends very weakly on the internuclear distance in the range of interest.

The ICD widths were computed using the Fano-Stieltjes method, with the bound and continuum part of the corresponding resonance state constructed using the extended ADC(2) scheme for the one-particle propagator.[26] For this purpose, we used on each atom an effective core potential (ECP) with $4s$, $4p$, $4d$, and $1f$ basis functions with 8 active valence electrons. The ECP was adjusted in energy to nonrelativistic and scalar relativistic energies.[27] The basis was further augmented by $8s$, $8p$, $8d$, $5f$, and $3g$ diffuse functions on the atomic centers and additional sets of $3s$, $3p$, and

TABLE I. Computed ICD widths of the ionization satellites used to obtain the ICD spectra. The values are given at the equilibrium interatomic distance R_e and at the inner turning point $R_{t.p.}$ whose position is shown in parentheses. The states for which $\Gamma(R_{t.p.})$ is missing are dissociative. *Note:* The decay widths of the two $Ar^+(3p^{-2}5s)Kr$ states could not be obtained within the present approach. Therefore, in order to compute the ICD-electron and KER spectra of these states, we used averages of the widths of the corresponding states of g- and u-symmetry in Ar_2.[13]

$Ar^+(3p^{-2}nl)Kr$ ionization satellite	Molecular term symbol	$\Gamma(R_e)$ (meV)	$\Gamma(R_{t.p.})$ (meV)
$3p^{-2}[^1D]4s\,^2D$	Σ^+	10.34	…
	Π	9.15	…
	Δ	4.91	9.71 (3.51 Å)
$[^3P]3d\,^2D$	Σ^+	5.46	20.34 (3.48 Å)
	Π	4.33	4.85 (3.88 Å)
	Δ	2.97	…
$[^1S]4s\,^2S$	Σ^+	14.81	…
$[^1D]3d\,^2D$	Σ^+	44.72	84.97 (3.44 Å)
	Π	34.95	…
	Δ	16.05	21.15 (3.44 Å)
$[^1D]3d\,^2P$	Σ^-	11.26	…
	Π	29.22	33.71 (2.87 Å)
$[^1S]3d\,^2D$	Σ^+	0.95	…
	Π	1.25	…
	Δ	3.06	18.89 (3.38 Å)
$[^3P]5s\,^2P$	Σ^-	1.48	12.71 (2.84 Å)
	Π	0.57	11.28 (3.00 Å)
$[^1D]5s\,^2D$	Σ^+	0.62	12.10 (2.90 Å)
	Π	0.21	4.43 (2.90 Å)
	Δ	0.44	3.83 (2.84 Å)
$[^1D]4d\,^2P$	Σ^-	0.67	12.26 (2.89 Å)
	Π	0.53	6.61 (2.91 Å)
$[^1D]4d\,^2D$	Σ^+	0.87	6.63 (2.91 Å)
	Π	0.36	16.67 (2.91 Å)
	Δ	0.60	5.28 (2.91 Å)
$[^1D]4d\,^2F$	Σ^-	0.33	5.88 (2.89 Å)
	Π	0.23	5.63 (2.91 Å)
	Δ	0.18	12.67 (2.91 Å)
	Φ	0.47	2.60 (2.89 Å)

$4d$ functions on 5 ghost centers on the interatomic axis. The diffuse functions were specifically designed for the computation of Rydberg and continuum states.[28] The computed decay widths of the ionization satellites of interest at the ArKr equilibrium distance and at the turning points of the corresponding PECs are listed in Table I.

The potential curves and decay widths serve as input for the nuclear dynamics calculation. The nuclear vibrational motion during the ICD step can be described by wave packets propagating on the PECs of the decaying and final states. The time-evolution of the nuclear wave packets was computed using the Lanczos-Arnoldi algorithm[29] as implemented in the multi-configuration time-dependent Hartree (MCTDH) package.[30,31] The propagation times for different decaying states vary between 700 fs and 200 ps. The ICD-electron spectra were computed from the final nuclear wave packets as follows. First, the kinetic energy distributions of the

emitted electrons following the decay in a particular channel were obtained from the nuclear wave packets on the corresponding final state at large times, when the decay is essentially complete[32]

$$\sigma_{f_k}^i(E_e) = \lim_{t \to \infty} \langle \Psi_{f_k}^i(E_e, t) | \Psi_{f_k}^i(E_e, t) \rangle.$$

The ICD electron spectrum of a particular decaying state was then computed as a sum of the partial intensities $\sigma_{f_k}^i(E_e)$, which correspond to all possible decay channels

$$\sigma_i(E_e) = \sum_k \sigma_{f_k}^i(E_e).$$

The kinetic energy distributions of the ionic fragments (KER spectra) were evaluated from the ICD-electron spectra using the mirror-image principle

$$\sigma_{KER}^i(E_{KER}) = \sigma_{ICD}^i(E_i(R_e) - E_f(\infty) - E_e),$$

where E_{KER} is the kinetic energy of the nuclei, $E_i(R_e)$ is the electronic energy of the decaying state at R_e, $E_f(\infty)$ is the asymptotic energy of the final states (the same for all 18 channels in our case).

The total ICD-electron and KER spectra of a cascade initiated by a particular core excitation were calculated as weighted sums of the spectra belonging to the ionization satellites populated in the resonant Auger step. Finally, to account for the experimental resolution,[11] the total ICD-electron and KER spectra were convolved with Gaussians of FWHM 1.24 eV and 0.64 eV, respectively.

III. THE ROLE OF THE PARTNER ATOM

To understand how the energy distributions of the emitted particles in the ICD process depend on the nature of the neighboring atom, we first consider the atomic properties of Kr compared to Ar. Krypton is a "softer" atom (see, e.g., Ref. 33 for a definition of "soft" and "hard" atoms). As such, it has larger atomic and van der Waals radii (1.89 Å compared to 1.79 Å for Ar[34]), larger polarizability (17.07 a.u. compared to 11.22 a.u. for Ar[35]), and lower ionization potential (14.00 eV compared to 15.76 eV for Ar[25]), the latter two quantities being inversely proportional.[36]

Let us now consider how the PECs of the states of interest are influenced by the presence of a "softer" neighbor. The positions of the peaks in the ICD-electron and KER spectra are determined by the ground-state equilibrium distance R_e, the positions of the inner turning points of the decaying states PECs, the ratios between the characteristic vibrational periods and the ICD lifetimes of the decaying states, as well as the shape of the final states PECs.[13] As a result of the higher polarizability and larger van der Waals radius of Kr, the ground-state PEC of ArKr (Fig. 1, lower panel) is deeper, $D_e = 13.3$ meV, and its minimum is shifted to larger interatomic distances ($R_e = 3.94$ Å) compared to the ground-state PEC of Ar$_2$ ($R_e = 3.80$ Å).

The PECs of the initial ICD states are presented in the upper panel of Fig. 1. Due to the lower ionization potential of Kr, two more ionization satellites in ArKr become available for ICD compared to Ar$_2$, namely, Ar$^+$($3p^{-2}$[^1D]$4s\,^2D$)Kr
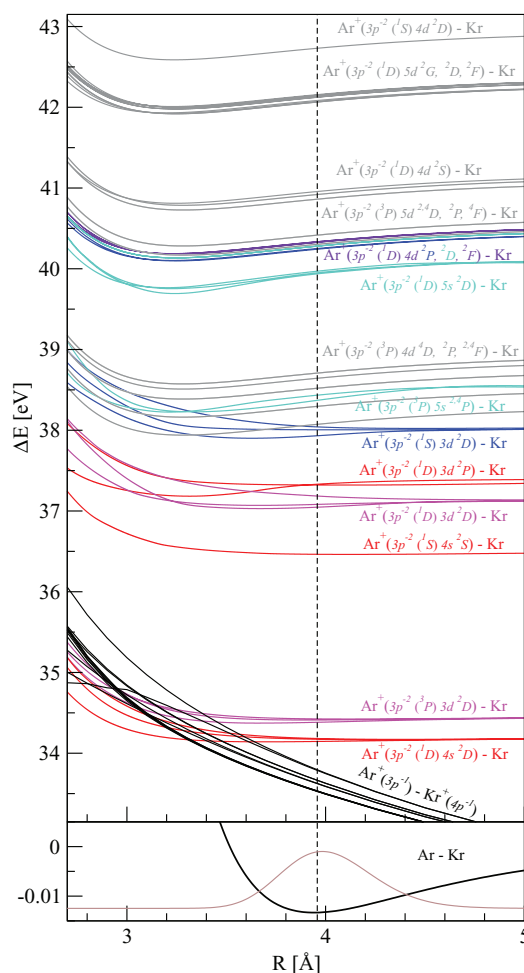
FIG. 1. Potential energy curves of ArKr: (lower panel) the ground-state PEC and ground-state wave packet density of ArKr; (upper panel) the black curves represent the final repulsive two-site dicationic states Ar$^+$($3p^{-1}$)Kr$^+$($4p^{-1}$); the red and pink curves are the lowest fast-decaying ionization satellites, the blue and violet curves represent the higher slow-decaying satellites (see Table I for the corresponding decay widths). The ionization satellites which were not included in the dynamics calculation, but are populated after the resonant Auger decay are shown in grey.

and Ar$^+$($3p^{-2}$[^3P]$3d\,^2D$)Kr. Thus, the initial ICD states form three groups lying in the energy ranges 34–35 eV, 36–39 eV, and above 39 eV. The ionization satellites belonging to a given group are expected to decay by emitting electrons of similar energies and, hence, contribute to the same peak in the total ICD-electron spectrum. Therefore, in the ICD-electron spectrum of ArKr one would expect three peaks, in contrast to the double-peak structure observed in the spectrum of Ar$_2$. The PECs of the low-lying ionization satellites (Ar$^+$($3p^{-2}$[^1D]$4s\,^2D$)Kr, Ar$^+$($3p^{-2}$[^3P]$3d\,^2D$)Kr, Ar$^+$($3p^{-2}$[^1S]$4s\,^2S$)Kr, Ar$^+$($3p^{-2}$[^1D]$3d\,^2D$)Kr, Ar$^+$($3p^{-2}$[^1D]$3d\,^2P$)Kr, Ar$^+$($3p^{-2}$[^1S]$3d\,^2D$)Kr) are shallow, with minima located between 3.32 and 5.09 Å and depths in the range between 31 and 217 meV. Their characteristic vibrational periods vary between 290 fs and 2.20 ps. The PECs of the remaining high-lying ICD states have different binding properties. They are deeper, with binding energies between 265 and 334 meV, and their minima are located at shorter internuclear distances 3.20–3.34 Å. Their characteristic

vibrational periods are between 280 and 290 fs, and generally tend to be shorter than those of the low-lying states. Due to the similar binding properties of the PECs of ArKr and Ar$_2$, the vibrational periods in ArKr do not significantly differ from the corresponding vibrational periods in Ar$_2$.

There are 12 two-site dicationic final states of the kind Ar$^+(3p^{-1})$Kr$^+(4p^{-1})$ (Fig. 1, upper panel). Their PECs are repulsive, behaving as R^{-1} at large interatomic distances. Compared to the corresponding PECs of Ar$_2$, the final states of ArKr are more repulsive at shorter internuclear distances due to the larger van der Waals radius of Kr. However, the difference is negligible and does not affect the positions of the peaks in the spectra.

Let us focus now on the decay widths of the ionization satellites included in the nuclear dynamics calculation (see Table I). The differences between the decay widths of the states converging to the same ionization satellites of Ar in ArKr and Ar$_2$ are of the order of 10%, which is within the error of the computational approach. Therefore, replacing Ar with Kr does not qualitatively change the ICD widths. We can conclude from this and from the above discussion of the vibrational periods that the division into fast- and slow-decaying states made in the case of Ar$_2$ also remains valid in the case of ArKr. The lowest-lying satellites correlating with Ar$^+(3p^{-2}3d, 4s)$Kr (except for the Ar$^+(3p^{-2}[^1S]3d\,^2D)$Kr state) are fast-decaying. Their decay lifetimes range between 29 and 443 fs, and are by an order of magnitude shorter than the typical vibrational periods (290 fs–2.20 ps). Consequently, the decay of these states takes place around R_e. The higher-lying ionized-excited states converging to Ar$^+(3p^{-2}5s, 4d)$Kr fall into the group of the slow-decaying states. Their ICD lifetimes at R_e range between 2.30 and 5.60 ps, and are by an order of magnitude longer than the typical vibrational periods (280–290 fs). Thus, the decay of these states is substantially affected by nuclear dynamics and predominantly happens close to the inner turning points $R_{t.p.}$ of the corresponding PECs (see Table I for their positions). A detailed description of the decay as well as the spectra of these two groups of states can be found in Ref. 13.

In order to illustrate the influence of the chemically "softer" neighbor on the ICD-electron spectrum, we compare the electron spectra of Ar$_2$ and ArKr, originating from the same core excitation, Ar$(2p_{3/2} \rightarrow 4s)$ (see Fig. 2). The resonant Auger decay of this state proceeds predominantly according to the strict spectator model, leading to the population of the fast-decaying Ar$^+(3p^{-2}4s)$ and Ar$^+(3p^{-2}3d)$ lowest satellites with 89% probability.[37] The remaining 11% of the populated states are the slow-decaying shake-up satellites Ar$^+(3p^{-2}5s)$ (see Table I in Ref. 37). We assume that the states populated in the dimer are the same as in the atom and their branching ratios are preserved as well (see Refs. 10 and 13).

Let us first compare the ICD-electron spectrum of Ar$_2$ which derives from the decay of the Ar$^+(3p^{-2}[^1S]4s\,^2S)$Ar, Ar$^+(3p^{-2}[^3P]5s\,^2P)$Ar, and Ar$^+(3p^{-2}[^1D]5s\,^2D)$Ar satellites with the portion of the ICD-electron spectrum of ArKr corresponding to the decay of the same Ar^{+*} states (see Figs. 2(a) and 2(b)). The Ar$_2$ spectrum possesses two peaks: one between 0.0 and 2.0 eV, attributed to the decay of
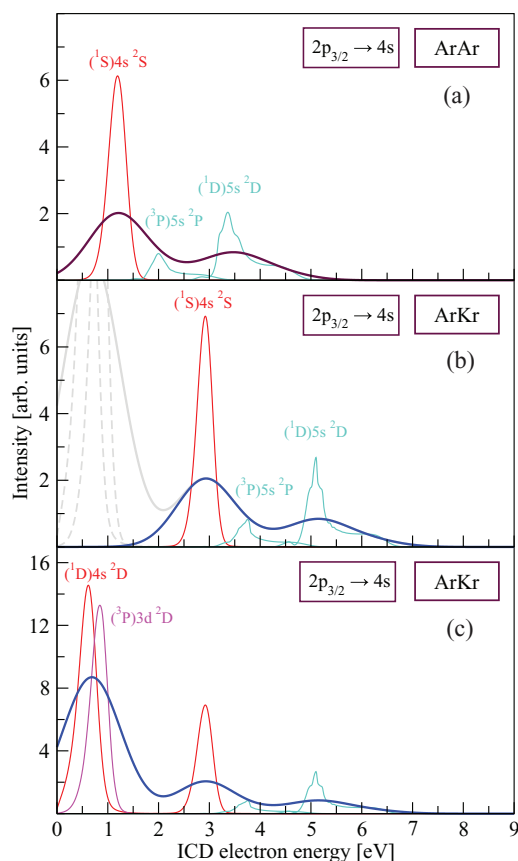
FIG. 2. Comparison between the ICD-electron spectra following the resonant Auger decay of the Ar$(2p_{3/2} \rightarrow 4s)$ core excitation in Ar$_2$ and ArKr. The total electron spectrum of Ar$_2$, shown in panel (a) (dark brown curve), is evaluated as a sum of the Ar$^+(3p^{-2}[^1S]4s\,^2S)$, Ar$^+(3p^{-2}[^3P]5s\,^2P)$, and Ar$^+(3p^{-2}[^1D]5s\,^2D)$ final resonant Auger states. The portion of the electron spectrum of ArKr (blue curve) originating from the decay of the same Ar^{+*} satellites is shown in panel (b). It has a similar structure and relative intensities of the peaks as that of Ar$_2$ (a), but due to the lower ionization potential of Kr, it is shifted to larger energies. The total ICD-electron spectrum of ArKr including all ICD-available states is depicted in panel (c). It exhibits a very intense peak at low energies originating from the decay of the two lowest satellites Ar$(3p^{-2}[^1D]4s\,^2D)$ and Ar$(3p^{-2}[^3P]3d\,^2D)$. All spectra shown in the figure are convolved with a Gaussian of FWHM 1.24 eV to account for the experimental resolution. The color scheme for the electron spectra originating from the different classes of satellites follows that of Fig. 1.

the Ar$^+(3p^{-2}[^1S]4s\,^2S)$Ar state, and a second peak between 2.5 and 5.0 eV, originating from the decay of the shake-up Ar$^+(3p^{-2}5s)$Ar states. The corresponding part of the ArKr spectrum (see Fig. 2(b)) possesses the same double-peak structure. However, due to the lower ionization potential of Kr compared to Ar, the energies of the final two-site dicationic states Ar$^+(3p^{-1})$Kr$^+(4p^{-1})$ decrease by the difference between the two ionization potentials, i.e., by 1.76 eV. Therefore, the respective part of the electron spectrum of ArKr is shifted to larger electron kinetic energies by approximately the same amount (see Figs. 2(a) and 2(b)). As we have discussed above, replacing Ar with Kr in the dimer causes small changes in the PECs and ICD widths of the states relevant for the peaks in question. These changes have in turn a minor effect on the structure of the corresponding portion of the ArKr spectrum, which can be seen by comparing the latter (Fig. 2(b)) with the Ar$_2$ spectrum (Fig. 2(a)).

Now let us consider the complete electron spectrum of ArKr (Fig. 2(c)). Due to the lower energies of the final two-site dicationic states, two more resonant-Auger final states become ICD-active in ArKr: $Ar^+(3p^{-2}[^1D]4s\,^2D)Kr$ and $Ar^+(3p^{-2}[^3P]3d\,^2D)Kr$. These two states are fast-decaying states (see Table I). Consequently, their decay occurs mostly at the equilibrium interatomic distance, producing a third peak at energies between 0.0 and 2.0 eV (see Fig. 2(c)). Its intensity is approximately four times higher than that of the second peak, due to the high Auger branching ratios of these two satellites. As a result, the percentage of the final resonant-Auger states undergoing ICD which is unusually low in Ar_2 (21%) grows to 67% in the case of ArKr for the $2p_{3/2} \rightarrow 4s$ parent core excitation. The total efficiency of the RA–ICD cascade thus increases by more than three times upon replacing of Ar with Kr as a neighbor.

The ICD-electron spectra corresponding to the other two parent core excitations considered in this work, namely, $Ar(2p_{1/2} \rightarrow 4s)$ and $Ar(2p_{3/2} \rightarrow 3d)$, are presented in Fig. 3. All three computed spectra possess three peaks originating from the decay of the three energetically separated groups of satellite states (Fig. 1). The lowest-energy peak (0.0–2.0 eV) originates from the decay of the $Ar^+(3p^{-2}[^1D]4s\,^2D)Kr$ and $Ar^+(3p^{-2}[^3P]3d\,^2D)Kr$ states, which are not available for ICD in Ar_2 due to the higher ionization potential of Ar. This peak has a high relative intensity in the spectra corresponding to the $Ar(2p_{3/2,\,1/2} \rightarrow 4s)$ parent core excitations, due to the high probability of populating these satellites in the RA decay (46% in the case of the $2p_{3/2} \rightarrow 4s$ excitation and 44% in the case of the $2p_{1/2} \rightarrow 4s$ excitation). In the spectrum corresponding to the $2p_{3/2} \rightarrow 3d$ core excitation, this peak is weak, since the population of the respective satellite states is only about 2%. The second peak in all three spectra is located between 2.0 and 4.5 eV. It is produced by ICD of the satellite states in the energy range 36.5–39.0 eV (see Fig. 1). The third peak is located at energies above 4.5 eV. It is attributed to the ICD of the higher Rydberg states of energies above 39.5 eV (see Fig. 1). Its high intensity in the spectrum originating from the $Ar(2p_{3/2} \rightarrow 3d)$ parent core excitation is a result of strong shake-up processes in the resonant Auger step. The two peaks at higher energy are virtually identical with the respective Ar_2 electron spectra since they originate from ICD of the states correlating with the same Ar satellites in both dimers (see Fig. 1, states of energies above 36.0 eV). The peaks in the spectra of ArKr are shifted to higher energies by approximately 1.76 eV relative to the spectra of Ar_2 due to the lower ionization potential of Kr. The availability of additional ICD-active states in ArKr increases the ICD yield by approximately a factor of 3 in the case of the $2p_{3/2,\,1/2} \rightarrow 4s$ parent states, whereas the yield in the case of the $2p_{3/2} \rightarrow 3d$ core excited state remains almost unaltered.

The computed KER spectra of the three core excited states are presented in Fig. 4. The KER spectra of ArKr are rather similar to those of Ar_2 (see Fig. 5 in Ref. 13). The two peaks manifest that the decay occurs at two different internuclear separations: the ground-state equilibrium distance $R_e = 3.94$ Å and the inner turning points of the considered PECs (located between 2.84 and 3.00 Å for the satellites of inter-
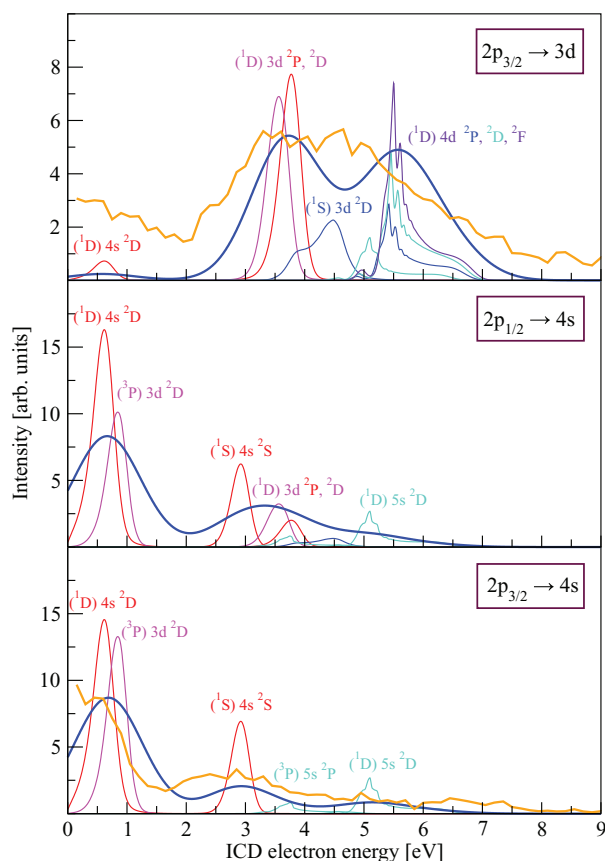
FIG. 3. ICD-electron spectra obtained in the RA-ICD cascade following $Ar(2p_{3/2} \rightarrow 4s)Kr$ (lower panel), $Ar(2p_{1/2} \rightarrow 4s)Kr$ (middle panel), and $Ar(2p_{3/2} \rightarrow 3d)Kr$ (upper panel) core excitations. The dark blue curves in all panels represent the total ICD spectra corresponding to the particular core excitation. Experimental data are available for the $Ar(2p_{3/2} \rightarrow 4s)Kr$ and $Ar(2p_{3/2} \rightarrow 3d)Kr$ excitation (orange curves).[11] In order to compare the experimental spectra with the theoretical ones, the latter were convolved using a Gaussian of FWHM 1.24 eV and the spectra were scaled such that the intensities of the most intense peaks coincide. The electron spectra resulting from the decay of the individual satellites contributing to the total spectrum of each core excitation are also presented (the color scheme follows that of the PECs in Fig. 1).

est). Thus, all fast decaying states contribute to the peak at lower energies (2.5–4.2 eV), whereas the high-energy peak (4.2–6.0 eV) is produced by the slow-decaying states. The corresponding low-energy peaks in the KER spectra of ArKr are shifted to lower kinetic energies by about 200 meV compared to their positions in the Ar_2 spectra. This is due to the larger ground-state equilibrium distance of ArKr. The higher peaks in the KER spectra of ArKr are also shifted to lower kinetic energies compared to Ar_2 because the inner turning points of the respective PECs are located at larger internuclear distances in the case of ArKr.

The available experimental ICD-electron and KER spectra[11,14] are shown in Figs. 3 and 4 as thick orange lines. As one can see from the figures, there is a very good correspondence between the computed and the experimental spectra. The calculations reproduce the number of peaks and their relative intensities. The discrepancies concern mainly the positions of the peaks, being larger for the higher-energy peaks which originate from the slow-decaying states. The deviations of the computed ICD-electron and KER spectra from the
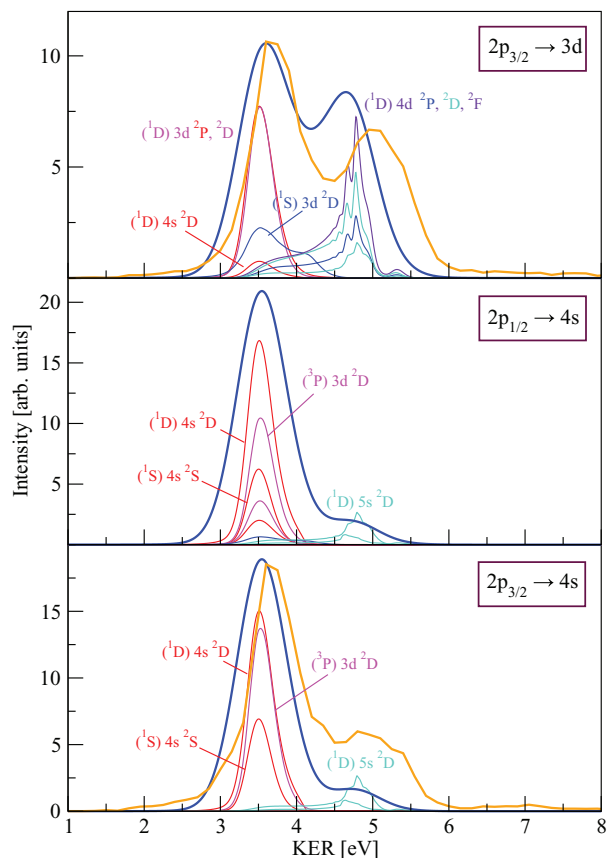
FIG. 4. KER spectra obtained in the RA-ICD cascade following Ar($2p_{3/2}$ → $4s$)Kr (lower panel), Ar($2p_{1/2}$ → $4s$)Kr (middle panel), and Ar($2p_{3/2}$ → $3d$)Kr (upper panel) core excitations. The spectra are obtained using the mirror-image principle. The dark blue curves in all panels represent the KER spectra corresponding to the particular core excitation. The orange lines are the available experimental KER spectra for the Ar($2p_{3/2}$ → $4s$)Kr and Ar($2p_{3/2}$ → $3d$)Kr core excitation.[11, 14] In order to compare the experimental spectra with the theoretical ones, the latter were convolved using a Gaussian of FWHM 0.64 eV and scaled such that the intensities of the most intense peaks coincide. The KER spectra of the satellites contributing to the total spectrum of each core excitation are also presented (the color scheme follows that of the PECs in Fig. 1).

experimental ones are between 60 and 280 meV, and between 70 and 370 meV, respectively. The errors are comparable with those in the case of Ar$_2$ and have opposite signs in the ICD-electron and KER spectra due to energy conservation used in the mirror-image principle (see Figs. 3 and 4). The sources of the discrepancies between the theoretical and the experimental spectra are the accuracy of the potential curves (i.e., the values of the equilibrium distance, inner turning points, as well as the characteristic vibrational periods) and the decay widths. They are discussed in detail in Ref. 13 for Ar$_2$, but also remain valid in the case of ArKr.

An additional source of error for this system is the neglect of relativistic effects. The spin-orbit coupling in the final ICD states leads to the splitting of the Kr$^+$($4p^{-1}$ ^2P) multiplet into the Kr$^+$($4p^{-1}$ $^2P_{3/2}$) and Kr$^+$($4p^{-1}$ $^2P_{1/2}$) terms which differ by 0.67 eV at asymptotic distances. Moreover, it has been shown[38] that the relativistically corrected ICD decay rates may differ from the non-relativistic ones. Including the relativistic corrections might shift the position of the theoretical peak by up to a few hundred meV.

Finally, we would like to discuss briefly the effect of omitting some ICD states from the calculations (see Fig. 1 for the satellites in question, their PECs are shown in grey). The largest deviation from the experiment should be observed for the ICD spectra of the $2p_{3/2}$ → $3d$ parent state where the neglected satellites carry up to 30% of the intensity. The decay of the states below 40 eV would produce electrons with energies between 2.7 and 4.0 eV. The decay of the states in the energy range between 40 and 42 eV is expected to produce electrons of energies between 5.0 and 6.3 eV and, thus enhance the high-energy peak. The highest Rydberg states would decay emitting electrons of energies above 6.5 eV, which would account for the difference between the theoretical and experimental spectra in this region. All of the above mentioned states are slow-decaying and would contribute to the high-energy peak in the KER spectrum.

We would also like to mention that the electronic spectra corresponding to the $2p_{1/2}$ → $4s$ and $2p_{3/2}$ → $3d$ parent core excitations in ArKr have been previously estimated[8] using a simple model. In this model, the PECs of the most populated ICD states were approximated as horizontal lines positioned at the correct asymptotic energies. The final states were represented by repulsive R^{-1} curves. The electron spectra were obtained assuming vertical ICD transitions taking place at the equilibrium distance of the ground state R_e. In this simple model, the low-energy peak originating from the decay of the fast states is accurately described. However, the high-energy peak produced from the decay of the slow ICD states is shifted by about 1 eV to higher kinetic energies. This is due to the fact that the decay of these states is accompanied by nuclear dynamics and it actually occurs in the vicinity of the inner turning points of the corresponding PECs. The nuclear motion during the decay also influences the form of the peak. It is now skewed to the large kinetic energies compared to the Gaussian-like peak resulting from the simple model used in Ref. 8. In addition, due to the assumption that ICD is very fast, according to this model the KER spectrum would consist of a single peak. However, as both the present calculations and the experimental results show, the KER spectrum actually consists of two peaks indicating that the fast and slow decay occur at different internuclear separations.

IV. CONCLUSIONS

In this paper, we studied the effect of the neighboring atom on the ICD-electron and KER spectra produced in the resonant-Auger – ICD cascade. To this end, we simulated the ICD-electron and KER spectra corresponding to three core excitations of Ar in ArKr ($2p_{3/2}$ → $4s$, $2p_{1/2}$ → $4s$, and $2p_{3/2}$ → $3d$). In order to obtain the spectra, we computed fully *ab initio* the PECs of the initial and final ICD states, as well as the respective ICD widths. The theoretical spectra were found to be in good agreement with the available experimental results.[11, 14] To gauge the role of the neighboring atom, we compared the spectra of ArKr with the analogous spectra of Ar$_2$, which were previously reported in Ref. 13.

We found that substituting the neighboring rare-gas atom with a chemically "softer" one has several consequences. Due to the larger van der Waals radius of Kr, the ground-state

equilibrium distance R_e increases and the positions of the inner turning points $R_{t.p.}$ in the PECs of the decaying states shift to larger internuclear separations. The decay of the fast and slow ICD states happens mostly at R_e and $R_{t.p.}$, respectively. Replacing Ar with Kr does not lead to a significant change in either the characteristic vibrational periods of nuclear motion or the ICD lifetimes of the satellite states. Therefore, the same division into fast- and slow-decaying states as in the case of Ar_2 remains valid in ArKr. The larger van der Waals radius of Kr also results in more repulsive character of the final $Ar^+(3p^{-1})Kr^+(4p^{-1})$ states at shorter internuclear distances. Moreover, reducing the ionization potential of the neighbor by replacing Ar with Kr lowers the energies of the final states by approximately 1.76 eV.

We have seen that the ionization potential of the neighbor has the most pronounced effect on the ICD-electron and KER spectra. On one hand, lowering the final states energies leads to an increase in the energies of the emitted electrons. Comparing the ICD-electron spectra of ArKr and Ar_2, one notices that the peaks originating from the decay of the satellites correlating with the same ionized-excited states of Ar are shifted to higher energies in the case of ArKr. The shift corresponds to the difference between the ionization potentials of Ar and Kr, namely, 1.76 eV. On the other hand, additional final resonant-Auger states may become ICD-active. In the present example, these are $Ar^+(3p^{-2}[^1D]4s\,^2D)Kr$ and $Ar^+(3p^{-2}[^3P]3d\,^2D)Kr$. The fast decay of these states produces electrons of kinetic energies between 0 and 2 eV. The increase in the number of available ICD states leads to an overall rise in the ICD yield. The increase is insignificant in the case of the $2p_{3/2} \rightarrow 3d$ core excitation due to the low probability of populating these states (only 2%). However, in the case of the $2p_{3/2,\,1/2} \rightarrow 4s$ core excitations the efficiency increases more than three times compared to Ar_2.

The KER spectra of ArKr possess the same double-peak structure as those of Ar_2, indicative of fast and slow decay taking place at two different internuclear separations. Due to the larger R_e and $R_{t.p.}$ of ArKr compared to Ar_2, the KER spectra are shifted to lower kinetic energies. In the case of ArKr, the relative intensity of the lower-energy peak compared to the high-energy one is much larger due to the decay of the additional ICD states, which in the case of the $2p_{1/2,\,3/2} \rightarrow 4s$ core excitations form up to 70% of the available ICD states.

In Ref. 8, we argued that one can control the location of the ICD process and the energies of the emitted ICD electrons using the RA–ICD cascade. As can be seen from the present results, the ICD-electron spectra are also very sensitive to the nature of the species being ionized in the ICD step. Therefore, we think that this property of the RA–ICD cascade can make it a spectroscopic tool which can be used alongside such well established methods as resonant Auger and near edge X-ray absorption fine structure (NEXAFS) spectroscopies.

ACKNOWLEDGMENTS

[1]L. S. Cederbaum, J. Zobeley, and F. Tarantelli, Phys. Rev. Lett. **79**, 4778 (1997).

[2]V. Averbukh, P. V. Demekhin, P. Kolorenč, S. Scheit, S. D. Stoychev, A. I. Kuleff, Y.-C. Chiang, K. Gokhberg, S. Kopelke, N. Sisourat *et al.*, J. Electron Spectrosc. **183**, 36 (2011).

[3]U. Hergenhahn, J. Electron Spectrosc. **184**, 78 (2011).

[4]H.-K. Kim, J. Titze, M. Schöffler, F. Trinter, M. Waitz, J. Voigtsberger, H. Sann, M. Meckel, C. Stuck, U. Lenz *et al.*, Proc. Natl. Acad. Sci. U.S.A. **108**, 11821 (2011).

[5]R. Santra and L. S. Cederbaum, Phys. Rev. Lett. **90**, 153401 (2003).

[6]Y. Morishita, X.-J. Liu, N. Saito, T. Lischke, M. Kato, G. Prümper, M. Oura, H. Yamaoka, Y. Tamenori, I. H. Suzuki *et al.*, Phys. Rev. Lett. **96**, 243402 (2006).

[7]K. Kreidi, T. Jahnke, T. Weber, T. Havermeier, X. Liu, Y. Morishita, S. Schössler, L. P. H. Schmidt, M. Schöffler, M. Odenweller *et al.*, Phys. Rev. A **78**, 043422 (2008).

[8]K. Gokhberg, P. Kolorenč, A. I. Kuleff, and L. S. Cederbaum, Nature (London) **505**, 661 (2014).

[9]P. O'Keeffe, E. Ripani, P. Bolognesi, M. Coreno, M. Devetta, C. Callegari, M. Di Fraia, K. C. Prince, R. Richter, M. Alagia *et al.*, J. Phys. Chem. Lett. **4**, 1797 (2013).

[10]M. Kimura, H. Fukuzawa, K. Sakai, S. Mondal, E. Kukk, Y. Kono, S. Nagaoka, Y. Tamenori, N. Saito, and K. Ueda, Phys. Rev. A **87**, 043414 (2013).

[11]M. Kimura, H. Fukuzawa, T. Tachibana, Y. Ito, S. Mondal, M. Okunishi, M. Schöffler, J. Williams, Y. Jiang, Y. Tamenori *et al.*, J. Phys. Chem. Lett. **4**, 1838 (2013).

[12]F. Trinter, M. S. Schöffler, H.-K. Kim, F. P. Sturm, K. Cole, N. Neumann, A. Vredenborg, J. Williams, I. Bocharova, R. Guillemin *et al.*, Nature (London) **505**, 664 (2014).

[13]T. Miteva, Y.-C. Chiang, P. Kolorenč, A. I. Kuleff, K. Gokhberg, and L. S. Cederbaum, J. Chem. Phys. **141**, 064307 (2014).

[14]K. Ueda and H. Fukuzawa, private communication (2014).

[15]S. Barth, S. Marburger, S. Joshi, V. Ulrich, O. Kugeler, and U. Hergenhahn, Phys. Chem. Chem. Phys. **8**, 3218 (2006).

[16]E. Fasshauer, M. Förstel, S. Pallmann, M. Pernpointner, and U. Hergenhahn, New J. Phys. **16**, 103026 (2014).

[17]P. Piecuch, S. A. Kucharski, K. Kowalski, and M. Musiał, Comput. Phys. Commun. **149**, 71 (2002).

[18]K. Raghavachari, G. W. Trucks, J. A. Pople, and M. Head-Gordon, Chem. Phys. Lett. **157**, 479 (1989).

[19]D. E. Woon and T. H. Dunning, Jr., J. Chem. Phys. **98**, 1358 (1993).

[20]A. K. Wilson, D. E. Woon, K. A. Peterson, and T. H. Dunning, Jr., J. Chem. Phys. **110**, 7667 (1999).

[21]B. R. Brooks and H. F. Schaefer, J. Chem. Phys. **70**, 5092 (1979).

[22]B. R. Brooks, W. D. Laidig, P. Saxe, N. C. Handy, and H. F. Schaefer III, Phys. Scr. **21**, 312 (1980).

[23]The diffuse s and d, and the compact d functions were generated as an even tempered sequence from the most diffuse s and d, and the most compact d basis functions with exponents $\xi = \alpha\beta^l$, where α is the exponent of the previous function, $\beta = 10$ and $l = 0.5$ for the compact exponent, $\beta = 10$ and $l = -0.5, -1$ for the diffuse exponents.

[24] T. Miteva, S. Klaiman, E. V. Gromov, and K. Gokhberg, J. Chem. Phys. **140**, 203420 (2014).

[25] A. Kramida, Y. Ralchenko, J. Reader, and N. A. Team, *NIST Atomic Spectra Database (version 5.1)* (National Institute of Standards and Technology, Gaithersburg, MD, 2013), URL: http://physics.nist.gov/asd.

[26] V. Averbukh and L. S. Cederbaum, J. Chem. Phys. **123**, 204107 (2005).

[27] A. Nicklass, M. Dolg, H. Stoll, and H. Preuss, J. Chem. Phys. **102**, 8942 (1995).

[28] K. Kaufmann, W. Baumeister, and M. Jungen, J. Phys. B **22**, 2223 (1989).

[29] W. T. Pollard and R. A. Friesner, J. Chem. Phys. **100**, 5054 (1994).

[30] H.-D. Meyer, U. Manthe, and L. S. Cederbaum, Chem. Phys. Lett. **165**, 73 (1990).

[31] H.-D. Meyer, G. A. Worth, M. H. Beck, A. Jäckle, U. Manthe, M. Ehara, A. Raab, M.-C. Heitz, S. Sukiasyan, C. Cattarius *et al.*, *The MCTDH Package, Version 8.4*, see http://mctdh.uni-hd.de/.

[32] E. Pahl, H.-D. Meyer, and L. S. Cederbaum, Z. Phys. D **38**, 215 (1996).

[33] R. G. Parr and R. G. Pearson, J. Am. Chem. Soc. **105**, 7512 (1983).

[34] M. Mantina, A. C. Chamberlin, R. Valero, C. J. Cramer, and D. G. Truhlar, J. Phys. Chem. A **113**, 5806 (2009).

[35] U. Hohm and K. Kerl, Mol. Phys. **69**, 803 (1990).

[36] K. I. Dmitrieva and G. I. Plindov, Phys. Scr. **27**, 402 (1983).

[37] J. A. de Gouw, J. van Eck, A. C. Peters, J. van der Weg, and H. G. M. Heideman, J. Phys. B **28**, 2127 (1995).

[38] E. Fasshauer, M. Pernpointner, and K. Gokhberg, J. Chem. Phys. **138**, 014305 (2013).